Photo-active chitosan-based hybrid films

Raquel Fernández [a*], Sebastian Bonardd [b], Itxaso Algar [a], Irati Barandiaran [a], Galder Kortaberria [a], Junkal Gutierrez [a,c], Agnieszka Tercjak [a]

[a] Group 'Materials + Technologies' (GMT), Department of Chemical and Environmental Engineering, Faculty of Engineering of Donostia-San Sebastian, University of Basque Country (UPV/EHU), Plaza Europa 1, 20018, Donostia-San Sebastian, Spain.

[b] Center of Applied Nanotechnology, Faculty of Science, Universidad Mayor, Camino Pirámide 5750, 8580745, Santiago, Chile.

[c] Faculty of Engineering of Vitoria-Gasteiz, University of the Basque Country (UPV/EHU), C/ Nieves Cano 12, 01006, Vitoria-Gasteiz, Spain.

*Corresponding author

Abstract

Biodegradable films for food packaging have received increasing attention from the industry in recent years. Due to its extraordinary properties, chitosan has demonstrated to be an exceptional candidate for that kind of applications. In this study, chitosan-based films modified with an azopolymer and silver nanoparticles were prepared by solvent-casting. The quality and homogeneity of the samples was satisfactory and films with thicknesses of the order of 25 μm and of various sizes, with diameters ranging from 5 to 15 cm, were obtained. The developed hybrid films were characterized by several experimental techniques including: atomic force microscopy, attenuated total reflectance-Fourier transformed infrared spectroscopy, thermogravimetric analysis, ultraviolet-visible spectroscopy and water contact angle measurements. In addition, the mechanical properties of the samples were investigated. Specifically, the tensile strength and the elastic modulus were enhanced in the films modified with azopolymer and silver nanoparticles. Moreover, the developed films showed reversible induced birefringence properties, indicating that they could be used for optical storage applications.

Keywords: chitosan, azopolymer, silver nanoparticles, films, characterization, induced birefringence, photo-active packaging

INTRODUCTION

Most of the food packaging developed nowadays is still obtained from petroleum-based polymers. However, consumer health and environmental pollution caused by the use of non-degradable petrochemical-based materials have motivated an increasing interest in food packaging materials based on biodegradable and natural polymers. In fact, the worldwide industrial production of biopolymers was of 3.5 billion tons in 2011 and it is expected to reach 12 billion tons in 2020 [1]. What is more, given the growing awareness for reducing pollution and plastic consumption, some companies have joined the eco-friendly initiative of laser printing in food. This allows to realize important savings when eliminating the paper labels that generate enormous waste. Therefore, taking all this into account, the main objectives of this work are the development of food bio-packaging, eliminating at the same time the paper labeling.

Regarding the material selected for that purpose, about 70 % of the Earth's surface is covered by the oceans, which correspond to about 90 % of the biosphere and offer a great source of novel compounds. Polysaccharides represent some of the most abundant bioactive substances in marine organisms. Among many polysaccharides that can be obtained from marine environment, chitin is the one that stands out due to its availability, as it is the second most abundant natural polymer after cellulose. Every year, approximately 100 billion tons of chitin are produced on the earth by crustaceans, mollusks, insects, fungi and related organisms [2]. Nevertheless, the applications of chitin are limited because of its poor solubility. Among the derivatives of chitin, chitosan (CH), which is a linear polymer obtained by the partial deacetylation of chitin, has attracted the attention of the scientists, due to its numerous applications in various fields, including food packaging [3-6]. This is consequence of the fact that chitosan, apart from being a biocompatible, biodegradable and non-toxic polymer, is also of particular interest due to its high antimicrobial activity [7] in combination with its excellent film forming ability [8].

Traditional polyolefins, such as polypropylene, polyethylene and polystyrene, are still extensively used due to their good chemical resistance, high impact resistance, plentiful supply and low cost. However, apart from not being biodegradable, they possess little inherent antimicrobial activity and are susceptible to bacterial contamination [9].

In order to evaluate the environmental load of chitosan films in comparison to the

environmental charge of conventional polypropylene films used nowadays as food packaging, Leceta *et al.* [10] carried out a comparative environmental assessment between the two different food packaging systems. They concluded that films based on polypropylene exhibited higher environmental impact than chitosan-based films in carcinogens and fossil fuels impact categories. The chitosan-based films manufacture was the stage that showed the highest impact because processing of these films is not currently optimized from an industrial point of view. Nonetheless, composting scenario for chitosan-based films exhibited a highly positive effect on the environment in comparison with the end of life scenarios for polypropylene films. In addition, chitosan-based films showed good functional properties for food packaging application, so that they could be a potential sustainable alternative since they turn a renewable by-product into a valuable material.

Chitosan can also be blended with synthetic polymers to develop films with combined properties [11]. As an example, the work developed by Martínez-Camacho *et al.* can be cited [12]. They obtained extruded films of low-density polyethylene, as polymer matrix, modified with 1-10 wt % of ethylene-acrylic acid copolymer, as adhesive, and 5 wt % of chitosan. These authors found that the addition of chitosan could enhance the degradability and bactericidal properties of the films. In a previous investigation of our group, we also combined chitosan with a synthetic polymer by electrostatic layer-by-layer self-assembly in order to obtain multilayer films with controlled architecture and properties [13].

On the other hand, in order to be able to remove paper labels in the food packaging, the material needs to have the ability to store information [14]. As far as this is concerned, azobenzene-containing polymers or azopolymers are well known as promising materials for optical data storage applications. This is possible thanks to the ability of azobenzene molecules to photo-orientate through optical induced *trans-cis-trans* isomerization cycles, when they are irradiated with linearly polarized light of appropriate wavelength. This photo-induced orientation gives rise to optical anisotropy or birefringence in azopolymers [15, 16]. Hence, in such polymeric systems a single domain could encode one bit by either being isotropic or birefringent, a difference that is easily probed optically. In addition, this optical process is reversible since data can be erased by changing the polarization of light from linear to circular [17].

Thus, in this paper, the first steps for the development of materials for photo-active food packaging are presented. In particular, chitosan-based films modified with a non-toxic azopolymer (PAZO) were prepared. The aim was to add the minimum content of PAZO needed to improve the thermal and mechanical properties of the films, as well as to obtain films with rewritable optical properties. Consequently, the maximum PAZO content used was 10 wt %. Besides, silver nanoparticles (Ag), which have demonstrated to have a broad antimicrobial activity [18], were added to the designed materials. Furthermore, the introduction of silver nanoparticles into polymer matrices containing azobenzene groups can enhance their photo-activity due to the localized surface plasmon resonance of these nanoparticles, especially when the azopolymer-containing film is irradiated at a wavelength close to their maximum absorption [19]. Finally, all the obtained films were characterized by several experimental techniques.

EXPERIMENTAL SECTION

Materials

Chitosan (CH) low molecular weight (M_v = 360.000 g/mol, 75 % deacetylation degree) was purchased from Sigma-Aldrich and purified by dissolution-filtration-precipitation method using HCl 0.5 M and NaOH 1 M aqueous solutions as solvent-precipitant pair. The azopolymer, poly[1-[4-(3-carboxy-4-hydroxyphenylazo)benzenesulfonamido]-1,2-ethanediyl, sodium salt] (PCBS), $AgNO_3$ and L-ascorbic acid were supplied by Sigma-Aldrich and used as received.

Films Preparation

The protocol for the film preparation is explained below. In a first step, protonated solid chitosan was formed by evaporating 5 mL of a 1 % m/v chitosan solution (1 % v/v acetic acid aqueous solution used as solvent). The solid obtained (50 mg) was milled into small pieces and stored for further use. On the other hand, a 2 % m/v aqueous solution of PCBS was prepared.

In a 15 mL glass vial, 10 mL of distilled water and 130 or 260 μL of PCBS solution (for CH95-PAZO and CH90-PAZO films preparation, respectively) were mixed. To this solution, 50 mg of protonated chitosan was slowly added and kept under vigorous stirring

during 24 h at room temperature. The homogeneous orange solutions were placed in petri dishes and allowed to dry at 45 ºC for 24 h in a ventilated incubator. Films obtained were immersed in a 1 M NaOH aqueous solution for 2 h followed by an 8 h washing process with Milli-Q water, changing water every 2 h, after which they were taken to dryness at 60 ºC during 24 h.

The synthesis of silver nanoparticles was performed through a two-step process in which, in a first stage, CH95-PAZO and CH90-PAZO films were immersed for 8 h in 50 mL of distilled water containing a certain amount of $AgNO_3$ (calculated to be 1 % w/w of Ag^+ with respect to the film mass), promoting the adsorption of Ag^+ ions onto films. After that, films were immersed in 100 mL of a 0.05 M L-ascorbic acid aqueous solution during 8 h in order to achieve a complete reduction of metal ions. Figure 1 shows an illustration of the chitosan-based films preparation method.

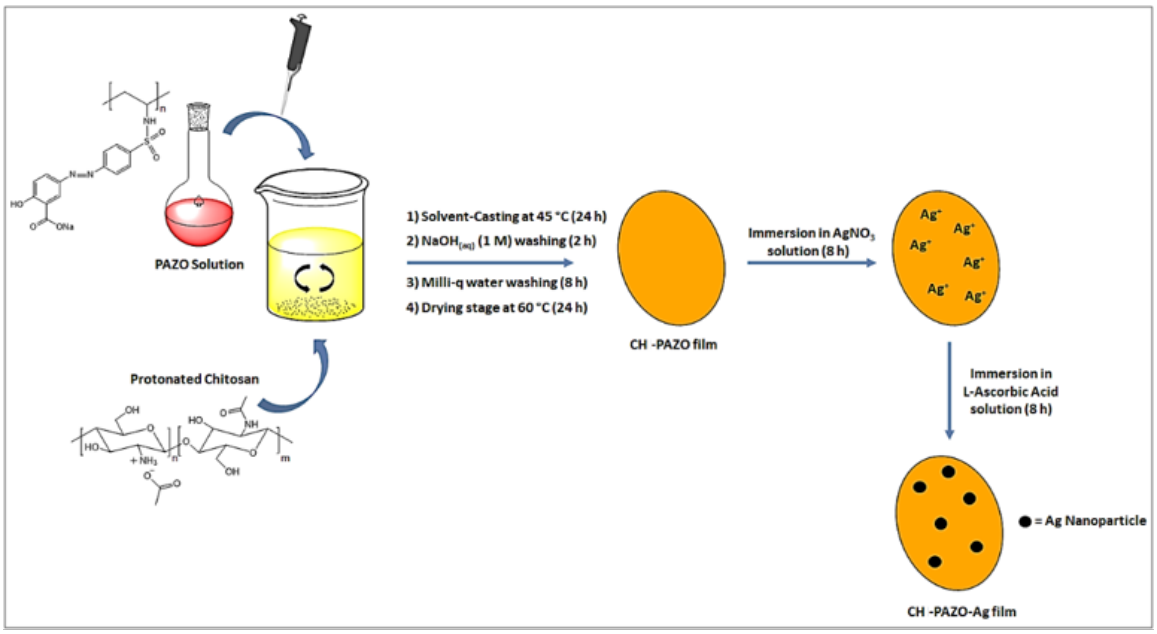

Figure 1. Preparation method of the solvent-cast films.

A summary of the exact composition and film thickness of the different samples is gathered in Table 1. Film thicknesses were calculated using a micrometer. The diameter of the films varied from 5 to 15 cm. Figure 2 shows images of the solvent-cast films.

Table 1. Composition and film thickness of the samples.

Sample	Chitosan (wt %)	Azopolymer (wt %)	Ag (wt %)	Thickness (mm)
CH	100	-	-	0.0303 ± 0.0082
CH95-PAZO	95	5	-	0.0145 ± 0.0041
CH95-PAZO-Ag [a]	94.1	4.9	1	0.0295 ± 0.0030
CH90-PAZO	90	10	-	0.0153 ± 0.0029
CH90-PAZO-Ag [a]	89.1	9.9	1	0.0296 ± 0.0029

[a] 1 % w/w of Ag with respect to the film mass

Films Characterization

Atomic force microscopy (AFM)

AFM images of the solvent-cast films were obtained with a NanoScope IIIa Multimode TM-AFM (Digital Instruments-Veeco) operating in tapping mode. The equipment contains an integrated silicon tip cantilever with a resonance frequency of 300 kHz. All the samples were placed on AFM metallic support for measurement and were conditioned at a temperature of 25 °C and a relative humidity of 50 % by means of saturated solution of potassium carbonate.

Attenuated total reflectance-Fourier transformed infrared spectroscopy (*ATR-FTIR*)

Infrared spectra of the samples were taken using a Nicolet Nexus 670 Fourier transform infrared spectrometer equipped with a single horizontal golden gate attenuated total reflectance cell. Spectra were recorded using a spectral width ranging from 600 to 4000 cm^{-1}, with 4 cm^{-1} resolutions and an accumulation of 32 scans.

Thermogravimetric analysis (TGA)

TGA of the samples was carried out using a TGA/SDTA 851e Mettler-Toledo equipment under nitrogen atmosphere at a heating rate of 5 ºC·min^{-1} from 25 to 600 ºC.

Ultraviolet-visible spectroscopy (UV-Vis)

The transparency of control chitosan and CH-PAZO with and without 1 wt % Ag films was observed in the wavelength range of visible light (200-800 nm) using a UV-Vis

spectrophotometer (Shimadzu UV-3600 UV-Vis-NIR). Each film was assessed in five replicates.

Water contact angle (WCA)

Static water contact angles of films were measured by the sessile drop method at room temperature using a Phoenix300 contact angle analyzer. The volume of the water droplet was 1.2 μL. The data presented of the measured contact angles are average values from measurements at five points chosen in the sample films.

Mechanical properties

The tensile strength, the elongation at break, and the elastic modulus of the films were calculated using an Instron (5976 30 KN) equipment, following ASTM D882 standard, with a rate of deformation of 1 mm/min. The thickness of the samples was determined using a micrometer, while the length and the width were 20 mm and 5 mm, respectively. For each value obtained, five samples were tested.

Optical storage experiments

Induced birefringence experiments were carried out at room temperature and under ambient conditions. The experimental setup used was similar to that previously reported [20]. Birefringence was induced in the films using a linearly polarized argon laser (writing beam) operating at 488 nm, which is within the range of absorption of the azopolymer. A low power He-Ne laser operating at 633 nm, which is out of the range of absorption of the azopolymer, was used as reading beam to measure the light intensity that is transmitted through the films between crossed polarizers. To achieve maximum signal, the polarization vector of the writing beam was set to 45º with respect to the polarization vector of the reading beam. The power of the writing beam used in the experiments was 20 mW on a spot of 0.4 mm^2 and the variation in the transmission of the reading beam was measured with a photodiode. The induced birefringence (Δn) was determined by measuring the reading beam transmission ($T = I/I_0$) according to:

$$\Delta n = (\lambda/\pi\, d)\, \sin^{-1}\, (I/I_0)^{1/2} \qquad (1)$$

where λ is the wavelength of the reading beam, d is the film thickness, I is the intensity of the reading beam after the second polarizer and I_0 is the transmitted intensity of the reading beam between parallel polarizers in absence of induced birefringence.

RESULTS AND DISCUSSION

At macroscopic scale, homogenous solvent-cast films of several sizes were obtained. The ones shown in Figure 2 presented a thickness of the order of 25 μm and a diameter of 5 cm. In addition, the yellowish colour that they took after the modification with azopolymer and the loss of transparency when the nanoparticles were incorporated can be observed.

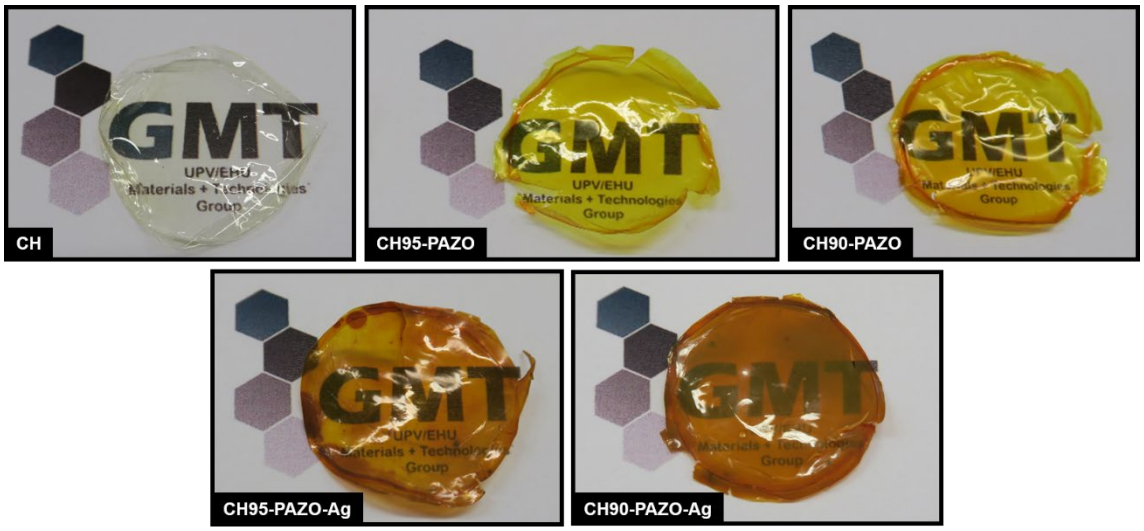

Figure 2. Photographs of the chitosan-based films.

To evaluate them at microscale, atomic force microscopy images were obtained, as can be seen in Figure 3. The morphology of neat CH and CH95-PAZO films was similar, but the increase of azopolymer content in CH90-PAZO gave rise to less homogeneous and rougher films.

Also, the incorporation of silver nanoparticles to the films had an effect on the morphology. Both CH95-PAZO-Ag and CH90-PAZO-Ag films showed homogenously dispersed bright dots of the silver nanoparticles, with a diameter of around 60 nm, on the surface of investigated films.

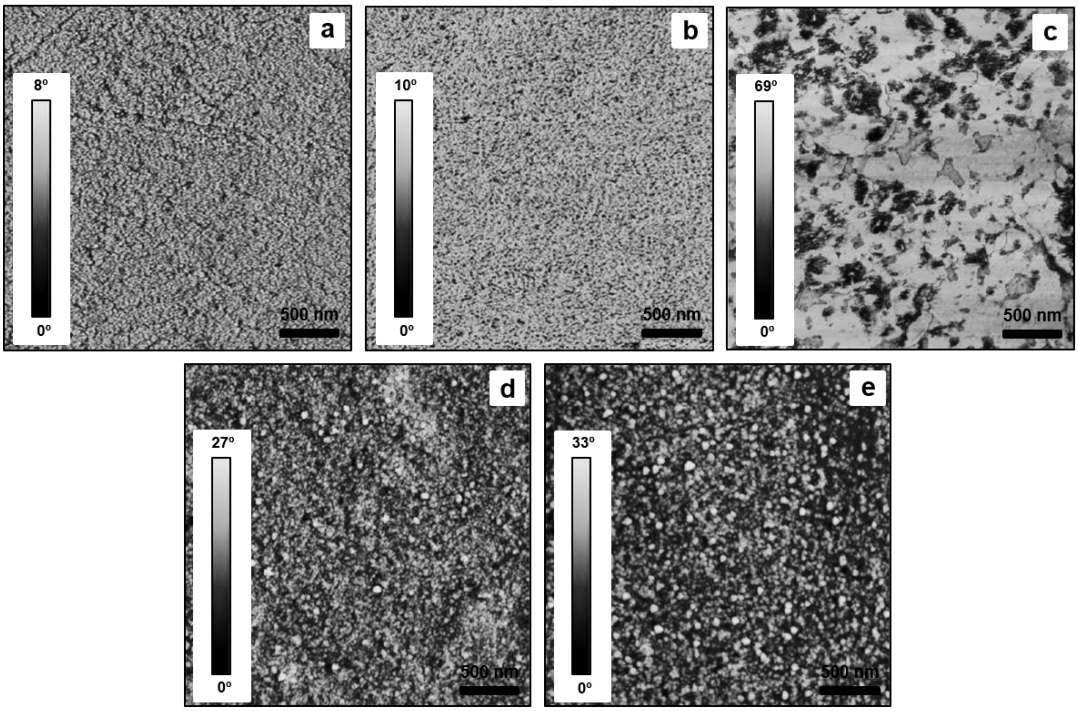

Figure 3. AFM phase images of: (a) CH, (b) CH95-PAZO, (c) CH90-PAZO, (d) CH95-PAZO-Ag and (e) CH90-PAZO-Ag (3 μm x 3 μm).

It is worth mentioning that an important aspect of hybrid nanocomposites is that both organic and inorganic materials do not show macrophase separation, in order to get a maximum homogeneity. As far as this is concerned, there were not found evidences of phase separation in the samples containing silver nanoparticles. Moreover, the addition of nanoparticles improved the microstructural distribution and homogeneity of the CH90-PAZO film. Thus, suggesting a high compatibility between PCBS solution and Ag nanoparticles, especially visible if compare morphology of CH90-PAZO and CH90-PAZO-Ag films.

All the chitosan-based films were also characterized by attenuated total reflectance-Fourier transformed infrared spectroscopy. In Figure 4, ATR-FTIR spectra are plotted.

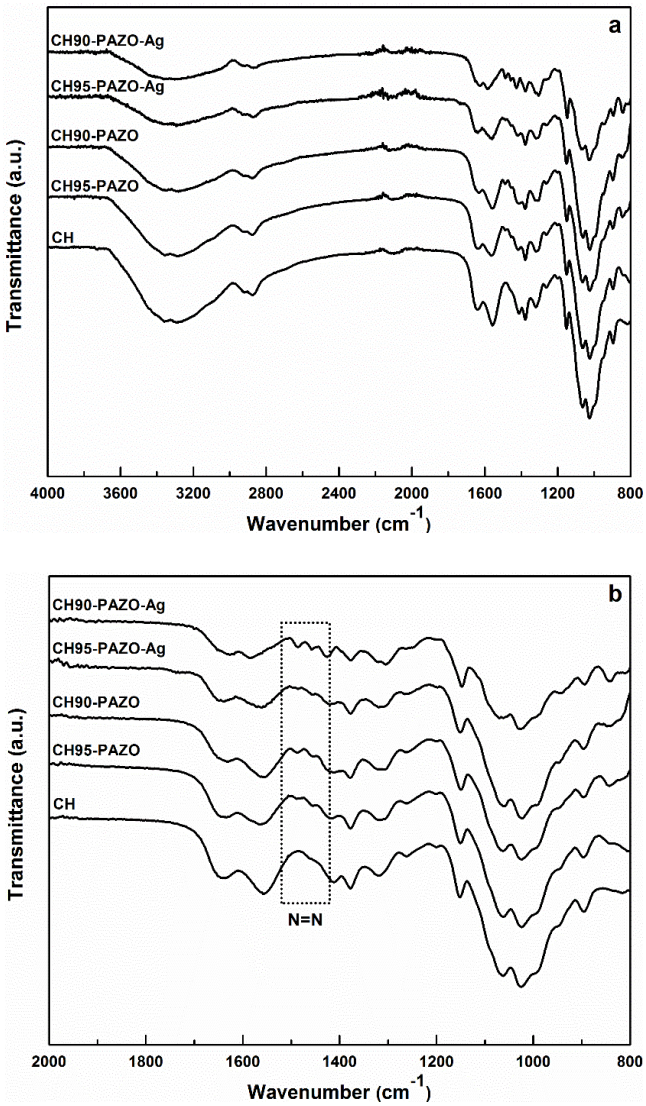

Figure 4. ATR-FTIR spectra of the samples within the range: (a) 4000-800 cm^{-1} and (b) 2000-800 cm^{-1}.

The stretching vibration of OH groups, overlapped with N-H stretching vibration, occurs in the 3315-3215 cm^{-1} region. The C-H stretching vibration is located at 2864 cm^{-1}. The band at 1650 cm^{-1} is related to C=O stretching vibration. At 1558 cm^{-1} appears the band attributed to N-H bending. The band located at 1414 cm^{-1} corresponds to -CH_2 bending vibration and the one at 1375 cm^{-1} is assigned to CH_3 groups symmetrical deformation. At 1150 cm^{-1}, the antisymmetric stretching vibration of C-O-C and the stretching vibration of C-N can be seen. The band related to C-O stretching vibration is observed at 1026 cm^{-1}. In the films modified with azopolymer the vibration associated with the stretching of N=N can be seen in the 1488-1427 cm^{-1} region.

Thermogravimetric analysis was carried out in order to analyze the weight loss of the samples as a function of temperature, as shown in Figure 5. In general, the shape of the thermograms is very similar, indicating that the thermal degradation followed an analogous pathway in all the samples. In the temperature range between 25 and 200 ºC, a process took place causing a first weight loss, which is also evidenced by a peak on the derivative curve. This weight loss may be attributed to water desorption, as was reported in previous thermal studies on chitosan [21, 22].

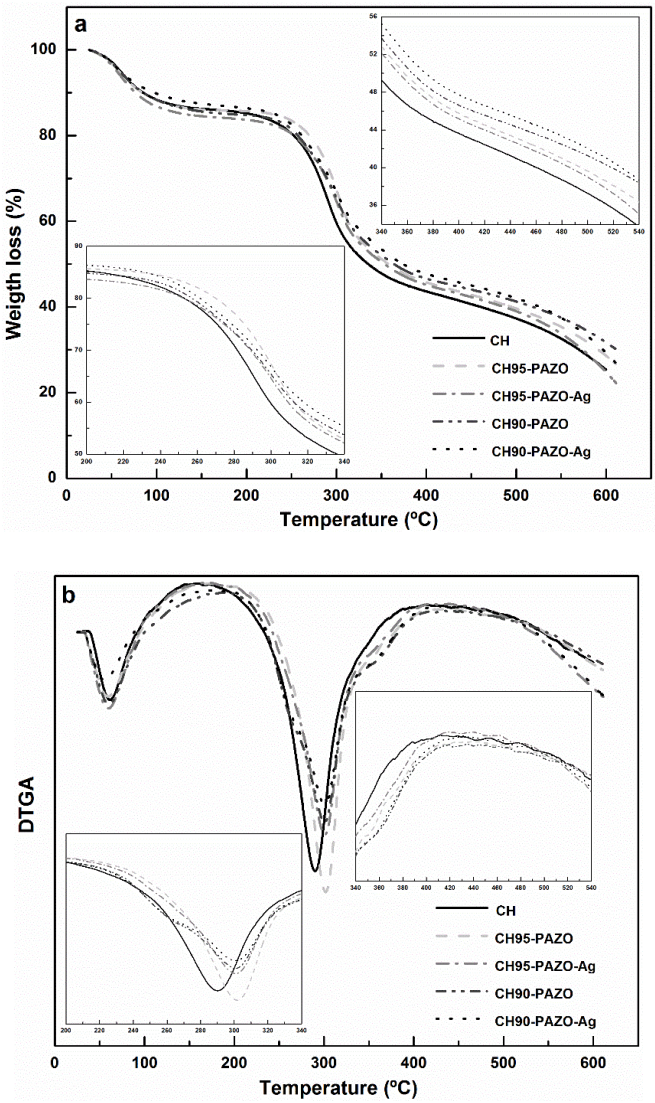

Figure 5. TGA results of the samples: (a) Thermogravimetric curves and (b) derivative curves.

Then, in the temperature range between 200 and 400 ºC, a dramatic weight loss process occurred. This process was ascribed to the degradation of chitosan, as well assessed in the literature [23-25]. It should be noted that, as revealed by the derivative curve, there was a slight shift of the chitosan degradation peak towards higher temperatures for the modified samples. Specifically, this peak was centered at 290 ºC for control chitosan, while for samples of modified chitosan it was centered at 302 ºC. This fact would indicate a delay of about 12 ºC in the thermal degradation thanks to the modification of chitosan. In addition, only modified samples exhibited two shoulders in the derivative curve. The first one in the temperature range between 225 and 280 ºC, and the second one between 340 and 400 ºC. These shoulders were more pronounced in samples with higher azopolymer content. Therefore, they were related to PAZO thermal degradation. However, there were no clear differences in the degradation process of the modified samples with and without silver nanoparticles. This could be due to the fact that the amount of silver nanoparticles was too small to be detected by the TGA equipment used.

The light-barrier properties of the films were determined by measuring their light absorption at wavelengths ranging from 300 to 700 nm. As shown in Figure 6, there was a clear variation in the samples optical absorbance with respect to control chitosan, especially in the range between 300 and 500 nm. The increase in absorbance at around 400 nm, exhibited by the modified films, may correspond to the electronic transition of azobenzene groups, responsible for the photo-isomerization, as well as for the yellowish colour of the samples.

When analyzing the results in more detail, it was observed that films containing silver nanoparticles showed a smaller difference in their response to light in the ultraviolet and visible range than films that only contained azopolymer, which showed a greater absorbance fall (or transmittance rise) in the range of visible light, with respect to the range of ultraviolet light.

Quantitatively, the transmittance of investigated films was compared at two different wavelengths, 400 and 600 nm. All the films were more opaque at 400 nm than at 600 nm. However, the transmittance of neat chitosan was higher than 80 % at both wavelengths, whereas for modified films it was less than 50 % at 400 nm and greater than that value at 600 nm. When comparing the modified samples with each other, it was found that CH95-PAZO was the most transparent film at the studied wavelengths. On the contrary, the most opaque film at 400 nm was CH90-PAZO, while at 600 nm the films containing

silver nanoparticle were more opaque. Consequently, around the absorbance wavelength of the azobenzene groups (400 nm), films with a higher azopolymer content were less transparent. At 600 nm, outside the absorbance range of the azopolymer units, the presence of silver nanoparticles became more important and the least transparent samples were those containing the nanoparticles.

In any case, neat chitosan was the most transparent film at all the range of wavelengths. Therefore, in general, modified films revealed better light-barrier properties.

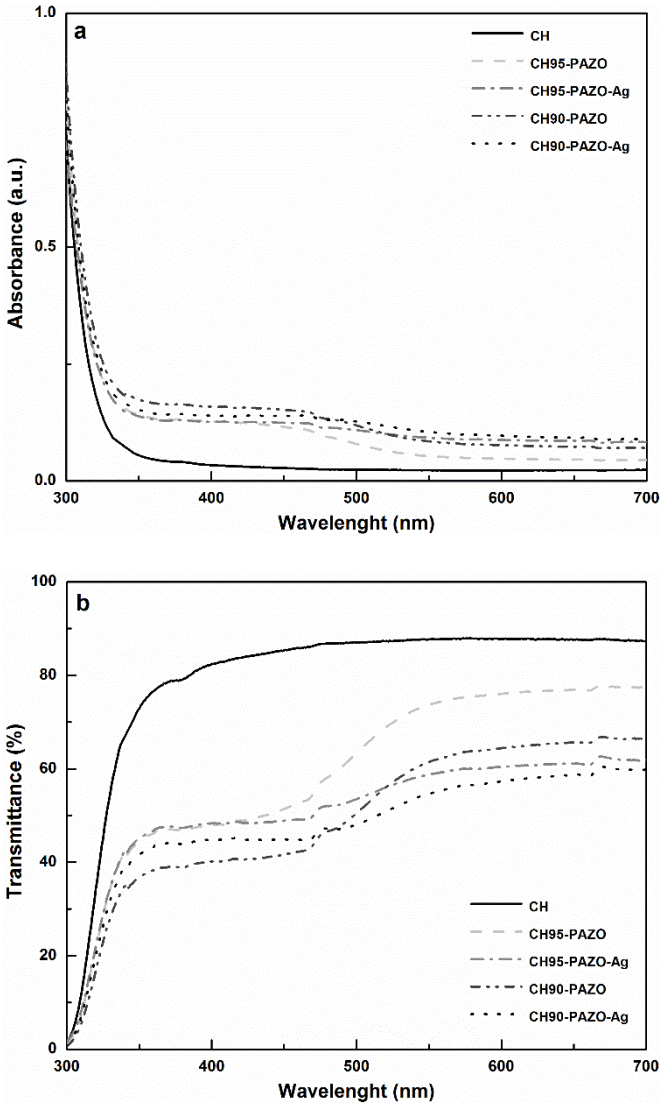

Figure 6. UV-Vis results of the samples: (a) Optical absorbance and (b) transmitance.

Surface wettability is a good indicator of the samples trend to absorb moisture; hence, can be used for estimating the water barrier properties of the films. Hydrophobicity of a

surface is typically determined by measuring the contact angle of a water droplet on the film surface, being higher when hydrophobicity of the film is higher [26].

Figure 7 presents the water drop size on the surface of the different films. The water contact angle of neat chitosan was increased from 65º to 77º, approximately, by the modification with azopolymer. Then, by adding silver nanoparticles, the WCA increased further, up to around 85º. Thus, according to the obtained data, the hydrophobicity was enhanced by the modification of the chitosan-based films with PAZO and silver nanoparticles.

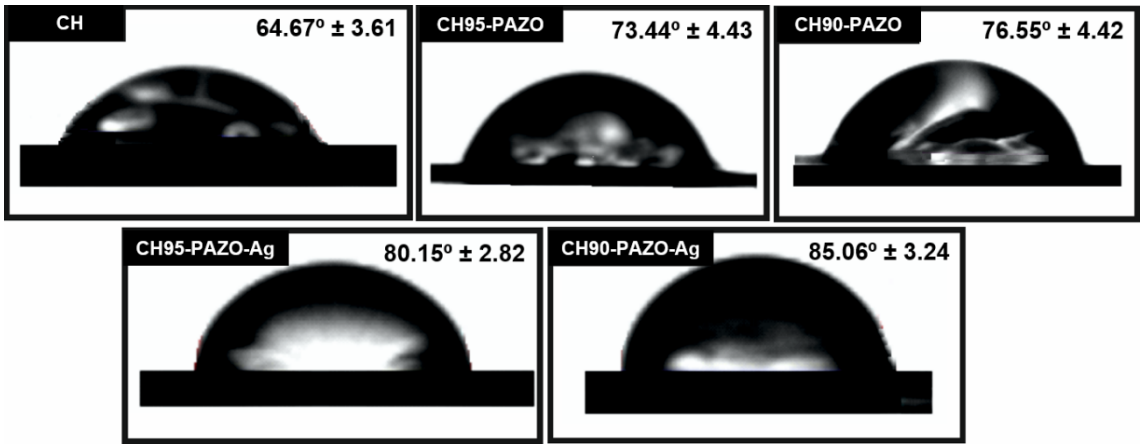

Figure 7. Images of the water drop size on the investigated films surface.

Of great interest is also the study of the mechanical properties of the obtained films. In this aspect, the elastic modulus, the tensile strength, and elongation at break of the films were calculated (Figure 8).

Regarding the elastic modulus and the tensile strength, these two properties clearly increased for CH95-PAZO and, even more, for CH95-PAZO-Ag with respect to control chitosan, but that trend was not so evident for CH90-PAZO and CH90-PAZO-Ag samples. In the case of CH90-PAZO, both the elastic modulus and the tensile strength decreased. This result could be connected to the microstructure presented by this sample (see Figure 3). Thanks to the addition of silver nanoparticles, the properties improved. In brief, to increase the rigidity and strength of the films, it would simply be necessary to modify them with 5 wt % azopolymer.

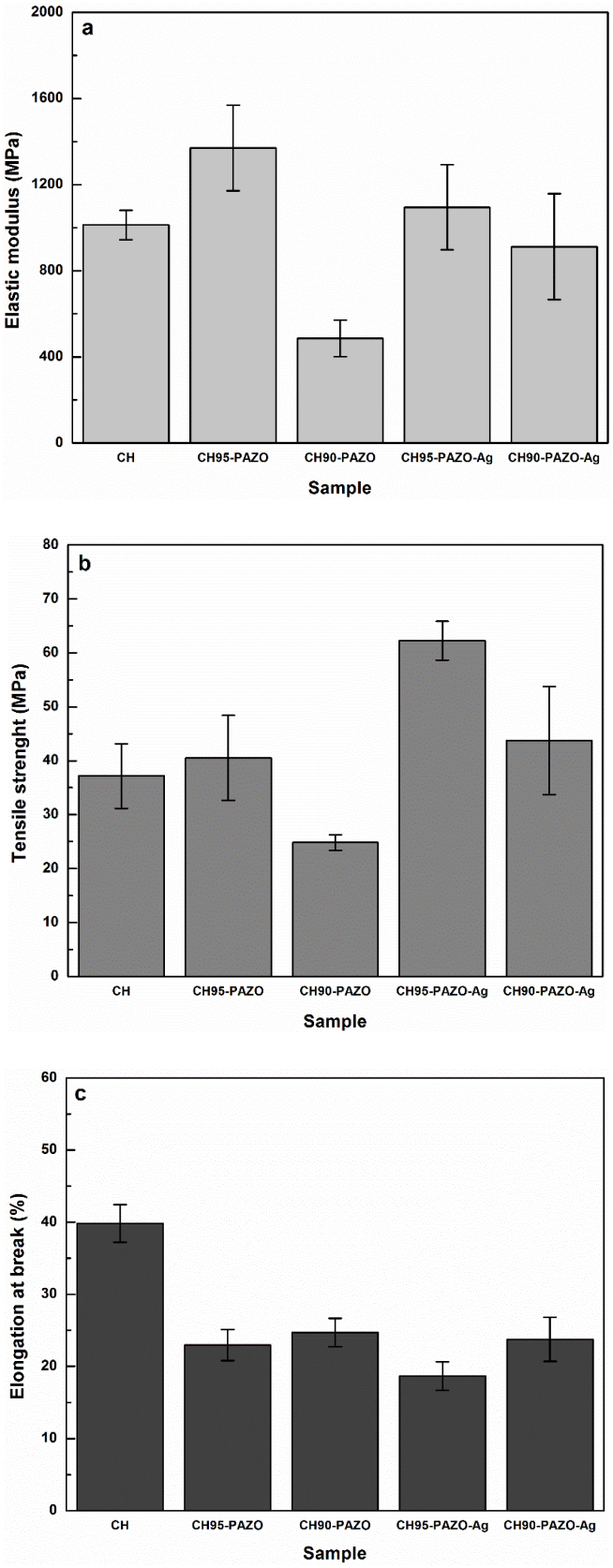

Figure 8. Mechanical properties of the samples: (a) elastic modulus, (b) tensile strength and (c) elongation at break values.

The elongation at break decrease by half for all modify films if compare to neat CH. Thus, the modification of the chitosan-based films with azopolymer and silver nanoparticles gave rise to less ductile films. Nonetheless, this property remained virtually almost unchanged regardless of the content of azopolymer and silver nanoparticles.

Finally, the reversible optical storage properties of the samples were studied. Some of the main characteristics a material requires to be used as an optical memory medium are high storage capacity (related to the maximum level of achievable birefringence, which corresponds to a writing mechanism), long-term stability (related to the remaining birefringence, which corresponds to a storing mechanism), and stability during several writing-erasing cycles.

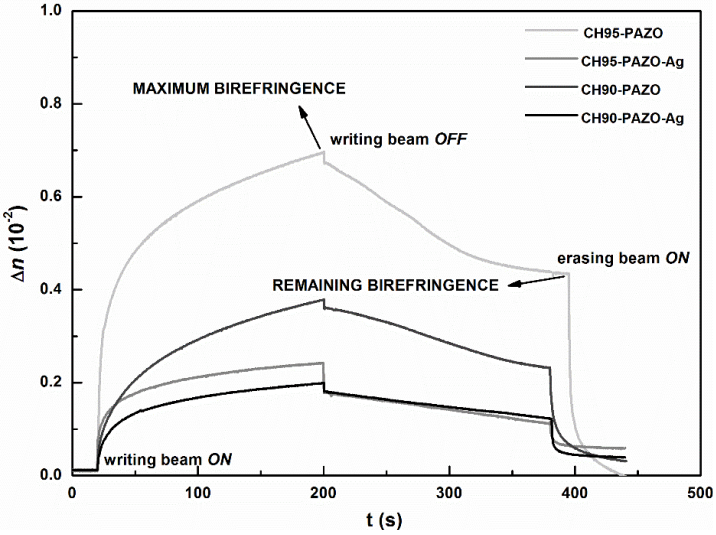

Figure 9. Writing-relaxing-erasing curves obtained for the chitosan-based films.

Figure 9 shows typical writing-relaxing-erasing curves obtained for the chitosan-based films. Initially, there was no transmission of the reading beam that continuously illuminated the samples, because azobenzene groups in *trans* form, which is the most stable configuration, were randomly distributed. When the samples were irradiated with linearly polarized light (writing beam), the reading beam was transmitted through them, placed between crossed polarizers, due to the optical anisotropy induced as a result of *trans-cis-trans* isomerizations, that led to the orientation of *trans* molecules perpendicular to the polarization vector of the writing beam. When the writing beam was turned *OFF*,

part of the photo-induced orientation was lost. In general, the birefringence might be preserved or not depending mainly on the nature of the azopolymer and its local environment [27, 28]. In this case, the birefringence was not completely conserved after writing with the linear polarized light, even though a significant amount of optically induced orientation was preserved. The erasing of the induced birefringence was achieved by irradiation with circularly polarized light (erasing beam), which completely removed the azobenzene groups orientation.

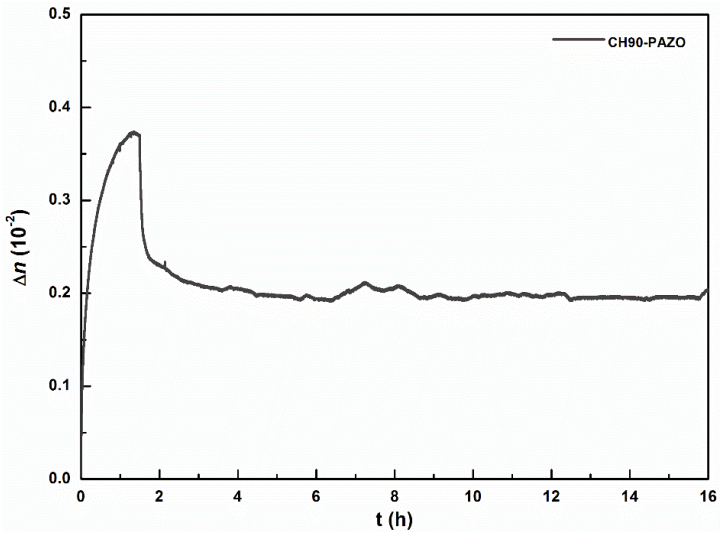

Figure 10. Writing and relaxing curves obtained for CH90-PAZO film.

In terms of storage capacity, the maximum level of birefringence, in the order of $0.72 \cdot 10^{-2}$, was achieved for CH95-PAZO film. However, assuming that Δn was due to the photo-induced orientation of the azobenzene groups, a larger number of photo-active units would generate a higher birefringence. According to this, CH90-PAZO film should present the highest Δn value. This result might be also related to the morphology shown by CH90-PAZO film at the microscale (see Figure 3). In this case, the addition of silver nanoparticles did not improved the birefringent properties of the films. Indeed, the level of birefringence achieved for both nanoparticles-containing films was lower than that for CH90-PAZO sample, which may indicate that silver nanoparticles hindered the azopolymer orientation.

As for the relaxing process, all the chitosan-based films exhibited a remaining

birefringence after 3 minutes of turning *OFF* the writing beam of around 60 %. The long-term stability was also studied. It was found that after more than 16 hours, the remaining birefringence was of the order of 50 %. The long-term relaxing curve obtained for a film of CH90-PAZO can be seen in Figure 10.

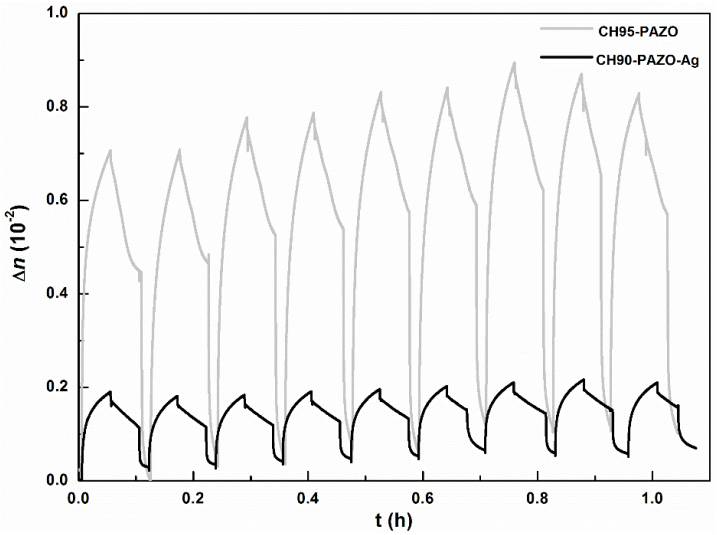

Figure 11. Successive writing-relaxing-erasing sequences obtained for CH95-PAZO and CH90-PAZO-Ag films.

Lastly but not least, the rewriting stability of the samples was also investigated. Figure 11 shows several writing-relaxing-erasing cycles for a film of CH95-PAZO and CH90-PAZO-Ag. During 1 hour experiment, after 9 successive writing-relaxing-erasing sequences the maximum and remaining birefringence values kept constant.

CONCLUSIONS

This paper presents the first steps towards the development of materials suitable for food bio-packaging applications with rewritable optical properties. In particular, chitosan-based films modified with azopolymer and silver nanoparticles were prepared by solvent-casting. All films showed adequate homogeneity at both macroscopic and microscopic levels. Specifically, it was found that the microstructure of CH90-PAZO film was the least homogeneous, a fact that affected directly on the properties of this film.

Regarding the thermal stability, a delay of about 12 ºC was observed in the degradation process of the modified films with respect to neat chitosan. Also, modified films revealed better light-barrier properties that neat chitosan in the range of wavelengths between 300 and 700. Furthermore, hydrophobicity was improved by the modification of the chitosan-based films with azopolymer and silver nanoparticles. As for the mechanical properties of the developed films, the results showed that to increase the rigidity and strength of the films, it would simply be necessary to modify them with 5 wt % PAZO.

Finally, the study about the reversible optical storage properties of the films indicated that the maximum level of birefringence achievable was in the order of $0.72 \cdot 10^{-2}$ for CH95-PAZO film. All the chitosan-based films presented a remaining birefringence of around 60 % after 3 minutes of turning *OFF* the writing beam, and of 50 % after more than 16 hours of turning *OFF* the writing beam. Besides, with regards to the rewriting stability of the films, after 9 successive writing-relaxing-erasing series the maximum and remaining birefringence values kept constant.

Acknowledgements

Financial support from Spanish Ministry of Science, Innovation and Universities and European Union (MICINN/FEDER and UE) in the frame of MAT2015-66149-P and PGC2018-097699-B-I00 projects is gratefully acknowledged. We also want to acknowledge the Basque Government for PIBA 2019-44 project and the University of the Basque Country for GIU18-216 research group. Moreover, we are grateful to the Macrobehavior-Mesostructure-Nanotechnology SGIker unit of UPV/EHU.

Data availability

The raw/processed data required to reproduce these findings cannot be shared at this time as the data also forms part of an ongoing study.

References

[1] K. Crouvisier-Urion, A. Lagorce-Tachon, C. Lauquin, P. Winckler, W. Tongdeesoontorn, S. Domenek, F. Debeaufort, T. Karbowiak, Food Chemistry 236 (2017) 120.

[2] N. Ruocco, S. Costantini, S. Guariniello, M. Costantini, Molecules 21 (2016) 55.

[3] P.K. Dutta, S. Tripathi, G.K. Mehrotra, J. Dutta, Food Chemistry 114 (2009) 1173.

[4] F.A. AlSagheer, M.A. Al-Sughayer, S. Muslim, M.Z. Elsabee, Carbohydrate Polymers 77 (2009) 410.

[5] E.S. Abdou, K.S.A. Nagy, M.Z. Elsabee, Bioresource Technology 99 (2008). 1359.

[6] K. Kurita, Marine Biotechnology 8 (2006) 203.

[7] N.R. Sudarshan, D.G. Hoover, D. Knorr, Food Biotechnol. 6 (1992) 257.

[8] F.S. Kittur, K.R. Kumar, R.N. Tharanathan, Z. Lebensm Unters Forsch. A, 206 (1998) 44.

[9] J. Lei, L. Yang, Y. Zang, Y. Wang, T. Ye, Y. Li, H. Deng, B. Li, Colloid Surf. B: Biointerfaces114 (2014) 60.

[10] I. Leceta, P. Guerrero, S. Cabezudo, K. de la Caba, J. Cleaner Prod. 41 (2013) 312.

[11] H. Wang, J. Qian, F. Ding, J. Agric. Food Chem. 66 (2018) 395.

[12] A.P. Martínez-Camacho, M.O. Cortez-Rocha, A.Z. Graciano-Verdugo, F. Rodríguez-Félix, M.M. Castillo-Ortega, A. Burgos-Hernández, J.M. Ezquerra-Brauer, M. Plascencia-Jatomea, Carbohydrate Polym. 91 (2013) 666.

[13] R. Fernández, C. Ocando, S. C. M. Fernandes, A. Eceiza, A. Tercjak, Biomacromolecules 15 (2014) 1399.

[14] R. Hagen, T. Bieringer, Adv. Mater. 13 (2001) 1805.

[15] H.M.D. Bandara, S.C. Burdette, Chem. Soc. Rev. 41 (2012) 1809.

[16] A. Natansohn, P. Rochon, Chem. Rev. 102 (2002) 4139.

[17] T.G. Pedersen, P.M. Johansen, H.C. Pedersen, J. Opt. A: Pure Appl. Opt. 2 (2000) 272.

[18] P.J. Rivero, A. Urrutia, J. Goicoechea, C. R. Zamarreño, F. J. Arregui, I. R. Matías, Nanoscale Research Letters 6 (2011) 305.

[19] R. Fernández, J. Gutierrez, A. Eceiza, A. Tercjak, RSC Adv. 5 (2015) 15740.

[20] R. Fernández, I. Mondragon, P. A. Oyanguren, M. J. Galante, React. Funct. Polym. 68 (2008) 70.

[21] X. Qu, A. Wirsén, A.C. Albertsson, Polymer 41 (2000) 4841.

[22] J.A. Ratto, T. Hatakeyama, R. B. Blumstein, Polymer 36 (1995) 2915.

[23] D. de Britto, S.P. Campana-Filho, Thermochim Acta 465 (2007) 73.

[24] C.G.T. Neto, J.A. Giacometti, A.E. Job, F.C. Ferreira, J.L.C. Fonseca, M.R. Pereira 62 (2005) 97.

[25] C.Q. Qin, Y.M. Du, L. Xiao, Polym. Degrad. Stab. 76 (2002) 211.

[26] D.Y. Kwok, A.W. Neumann, Adv. Colloid Interface Sci. 81 (1999) 167.

[27] R. Fernández, C. Ocando, A. Eceiza, A. Tercjak, Eur. Polym. J. 49 (2013) 3702.

[28] R. Fernández, H. Etxeberria, A. Eceiza, A. Tercjak, Eur. Polym. J. 49 (2013) 984.